Thiophene Adsorption and Activation on MoP(001), γ-Mo_2N(100), and Ni_2P(001): Density Functional Theory Studies

Jun Ren,[†] Chun-Fang Huo,[†] Xiao-Dong Wen,[†] Zhi Cao,[†] Jianguo Wang,*[,†] Yong-Wang Li,[†] and Haijun Jiao*[,†,‡]

State Key Laboratory of Coal Conversion, Institute of Coal Chemistry, Chinese Academy of Sciences, Taiyuan 030001, China, and Leibniz-Institut für Katalyse e.V. an der Universität Rostock, Albert-Einstein-strasse 29a, 18059 Rostock, Germany

Received: June 28, 2006; In Final Form: September 19, 2006

The adsorption and dissociation of thiophene on the MoP(001), γ-Mo_2N(100), and Ni_2P(001) surfaces have been computed by using the density functional theory method. It is found that thiophene adsorbs dissociatively on MoP(001), while nondissociatively on γ-Mo_2N(100) and Ni_2P(001). On MoP(001), the dissociation of the C−S bonds is favored both thermodynamically and kinetically, while the break of the first C−S bond on γ-Mo_2N(100) has an energy barrier of 1.58 eV and is endothermic by 0.73 eV. On Ni_2P(001) there are Ni_3P_2- and Ni_3P-terminated surfaces. On the Ni_3P_2-terminated surface, the dissociation of the C−S bonds of adsorbed thiophene is endothermic, while it is exothermic on the Ni_3P-terminated surface.

1. Introduction

Desulfurization of sulfur-containing organic molecules, especially thiophene and its derivatives as the common impurities in petroleum, is of considerable technological and fundamental interests due to the worldwide environmental regulations on the minimum sulfur level in fuel. The generally used process is hydrodesulfurization (HDS), which is normally based on molybdenum sulfide catalysts.[1] However, it has been shown that these sulfur-containing organic molecules are particularly difficult to desulfurize,[2] therefore extensive efforts have been focused on the search for more efficient HDS catalysts. It has been reported that transition metal carbide[3] and nitride[4] catalysts exhibit high activity and selectivity in many reactions including Fischer−Tropsch,[5] ammonia[6] and alcohol synthesis,[7] HDS,[8−10] and hydrodenitrogenation (HDN).[11,12] These new catalysts have the potential to replace the commercially used molybdenum sulfide catalysts in HDS reactions.[1,4,13,14] Recently, a number of studies has reported the HDN and HDS properties of bulk and supported metal phosphide catalysts for understanding the role of phosphorus in hydrotreating catalysts and for exploring the properties of a new class of materials—transition metal phosphides.[15−21] Given the need to develop highly efficient HDS catalysts for fulfilling the requirements for a lower sulfur level in fuel combined with the prospect of processing lower quality petroleum feedstock, further studies of phosphide-based hydrotreating catalysts are desired. Recent work has showed that MoP,[22−25] WP,[26] Ni_2P,[16,17,20,21,27−29] and Co_2P[30] are highly active for HDS and HDN of petroleum feedstock. Among them, Ni_2P/SiO_2 catalyst shows the highest HDS activity (HDS conversion of 99%) and is more efficient than $NiMoS/Al_2O_3$ (HDS conversion of 76%).[27] However, the key step of the desulfurization process, the C−S bond dissociation, is not well understood. Important prerequisites for an improved understanding are the knowledge about the initial adsorption modes of thiophene on these surfaces.

Thiophene has been widely used as the probe molecule in HDS studies both theoretically and experimentally. Previous work has focused on the interaction of thiophene with transition metals,[31] alloys,[32] oxides,[33] sulfides,[2,34] nitrides,[14,35] and carbides.[1,9] The bonding of thiophene on metal surfaces has been studied in detail.[31] Although metal nitrides and phosphides have higher activity in HDS, only a few experimental studies of thiophene adsorption on these surfaces are known.

In this work, we investigated thiophene adsorption on the MoP(001), γ-Mo_2N(100), and Ni_2P(001) surfaces at the density functional level of theory (DFT). Our goal is the understanding of thiophene activation on the surfaces of these novel catalysts.

2. Computational Methods

All calculations were done with the program package DMol[3] in Materials Studio of Accelrys Inc.[36] The physical wave functions are expanded in terms of accurate numerical basis set.[37] We used the double-numeric quality basis set with polarization function (DNP), while the density functional semicore pseudopotential (DSPP) was used for metals. The generalized gradient approximation (GGA) with the revised Perdew−Burke−Ernzerhof functional (RPBE)[38] was utilized for structure optimization and energy calculation. The RPBE functional usually gives absolute errors in adsorption energy of about 0.2 eV. A Fermi smearing of 0.0005 au (0.0136 eV) and a real-space cutoff of 5.5 Å were used to improve the computational performance. For numerical integration, we used the medium quality mesh, which has the following convergence criteria for structure optimization and energy calculation: (1) SCF of 1×10^{-5} au/atom; (2) energy of 2.0×10^{-5} au/atom; (3) maximum force of 4.0×10^{-3} au/Å; and (4) maximum displacement of 5.0×10^{-3} Å, respectively.

However, during our benchmark calculations we have found serious problems with the distribution of Mulliken charges on the clean MoP(001) surface by using the DSPP basis set. The calculated Mulliken charge of the surface Mo atom is negative

* Address correspondence to these authors. E-mail: jgwang@sxicc.ac.cn (J.W.) and haijun.jiao@ifok-rostock.de (H.J.).
[†] Chinese Academy of Sciences.
[‡] Leibniz-Institut für Katalyse e.V. an der Universität Rostock.

10.1021/jp0640474 CCC: $33.50
Published on Web 10/25/2006

TABLE 1: Computed Equilibrium Lattice Parameters of MoP, γ-Mo_2N, and Ni_2P

compds	$a = b$ (Å)	c (Å)
MoP	3.233 (3.223[a])	3.169 (3.191[a])
γ-Mo_2N	4.196 (4.163[b])	4.196 (4.163[b])
Ni_2P	5.887 (5.859[c])	3.346 (3.382[c])

[a] Taken from ref 42. [b] Taken from ref 43. [c] Taken from ref 44.

(−0.393e), while that of the subsurface P atom is positive (0.728e). The corresponding adsorption energy of thiophene (**1**) is unrealistically high (−3.87 eV). Faced with these problems, we have further carried out structure optimization and energy calculation by using an all-electron basis set. It should be noted that the calculated Mulliken charge of the surface Mo atom becomes positive (0.050e), while that of the subsurface P atom becomes negative (−0.085e), and this agrees with the reported literature values (0.045e vs. −0.077e).[39] The corresponding adsorption energy of thiophene is reduced (−2.80 eV). Further single-point energy calculations with an all-electron basis set on the DSPP optimized surface structure give nearly the same values, e.g., the surface Mo atom has positive charge (0.052e) and the subsurface P atom has negative charge (−0.092e), and the calculated adsorption energy of thiophene becomes −2.78 eV. On the basis of these agreements and the fact that full optimization with an all-electron basis set is much more expensive than single-point calculation, we have carried out single-point energy calculation on all systems studied in this paper, and the results with DSPP are given for comparison.

All unit cell optimizations were done with the CASTEP (Cambridge Sequential Total Energy Package) suite of programs,[36a] and ultrasoft pseudopotentials[40] were used to describe the ionic cores of MoP, γ-Mo_2N, and Ni_2P, and the Kohn−Sham one-electron states were expanded in a plane wave basis set up to 340 eV. Enough k-points were chosen for MoP ($9 \times 9 \times 8$), γ-Mo_2N ($6 \times 6 \times 6$), and Ni_2P ($5 \times 5 \times 8$). The exchange and correlation energies were described by the RPBE functional within the generalized gradient approximation. A Fermi smearing of 0.1 eV was utilized. Brillouin zone integration was approximated by a sum over special k-points chosen by using the Monkhorst−Pack scheme.[41] The computed equilibrium lattice parameters are given in Table 1.

MoP has a simple hexagonal WC-type structure with nonmetal-containing prisms stacked on top of each other. The calculated equilibrium lattice parameters of $a = 3.233$ Å and $c = 3.169$ Å are close to the experimental values of $a = 3.223$ Å and $c = 3.191$ Å.[42] In γ-Mo_2N, Mo atoms form a face center cubic crystal and N atoms occupy the largest interstitial octahedral sites. For bulk γ-Mo_2N, the calculated equilibrium lattice parameter of $a = 4.196$ Å agrees with the experimental value of about 4.163 Å.[43] Ni_2P adopts the hexagonal Fe_2P structure with the lattice parameters of $a = 5.859$ Å and $c = 3.382$ Å.[44] The calculated lattice parameters for bulk Ni_2P are $a = 5.887$ Å and $c = 3.346$ Å, in agreement with the experimental values and those determined by other authors.[45,46]

On the basis of the optimized unit cells as mentioned above, a p(3×3) unit cell with a slab of five layers for MoP(001) as well as four layers for γ-Mo_2N(100) and Ni_2P(001) was chosen to model thiophene adsorption. The slab was repeated periodically with 11 Å vacuum regions between the slabs. Only one thiophene molecule was adsorbed on one side of the slab with the coverage of 1/9 monolayer (ML) for comparison with experiments. At this coverage, lateral interactions of the adsorbed species should only reflect the interaction with the surface. A $2 \times 2 \times 1$ k-point sampling was used, and a test calculation for a larger k-point ($3 \times 3 \times 2$) was performed to make sure that there was no significant change in the calculated adsorption energies (0.04, 0.03, and 0.01 eV for MoP(001), γ-Mo_2N(100), and Ni_2P(001), respectively).

Adsorption energy was computed by subtracting the energies of gas-phase thiophene and the bare surface from the energy of the adsorbed system as shown in eq 1. With this definition, a negative E_{ads} means stable adsorption on the surface.

$$E_{ads} = E(\text{thiophene/surface}) - [E(\text{thiophene}) + E(\text{surface})] \quad (1)$$

3. Results and Discussion

3.1. Thiophene Adsorption on MoP(001). Figure 1a shows the Mo-terminated surface, which is very important for catalytic activity, because HDS reaction occurs mainly on Mo sites, as known from experiment.[47] The MoP(001) plane with a slab of five layers with alternating Mo and P layers is used, and the first three layers (2Mo + 1P) are allowed to relax, whereas the two bottom layers (1P + 1Mo) are fixed in their bulk positions.

Figure 2 shows five adsorption models on MoP(001), and the computed adsorption energies and structure parameters are tabulated in Table 2. In **1**, the sulfur atom stays around the bridge site, and the Mo−S distances are 2.443 and 2.465 Å. It should be noted that one of the C−S bonds is broken, as indicated by the long distance of 3.180 Å, and successively the carbon atom moves to the neighboring bridge site. In **2**, the sulfur atom caps over three Mo atoms with the Mo−S distances of 2.470−2.558 Å, and one of the C−S bonds also is broken, as indicated by the long distance of 3.318 Å. In **3**, thiophene adsorbs at the 3-fold Mo hollow site over one first layer P atom; and the sulfur atom caps over the Mo face center cubic site. The Mo−S distances are 2.637 to 2.660 Å, and the C−S bond lengths are 1.864 and 1.861Å, longer than that of 1.738 Å for free thiophene. In **4**, the thiophene ring adsorbs atop on one Mo atom with the C−S bond lengths of 1.864 and 1.879 Å. In **5**, the thiophene ring parallels the Mo face center cubic site, and the S atom adsorbs atop on the Mo site with the C−S bond lengths of 1.831 and 1.845 Å, respectively.

As given in Table 2, **1** with adsorption energy of −2.78 eV is most stable form, followed by **2** (−2.65 eV), while **3**−**5** are much less stable. In contrast to **3**−**5**, one of the C−S bonds in **1** and **2** is broken, indicating the stronger adsorption and activation. Such behavior on MoP(001) is also found on transition metals[31] and carbides.[1]

For comparison we also have computed the adsorption of thiophene on Mo(100). The optimized surface structures (3Mo + 2Mo) are shown in Figure 2 and the computed adsorption energies and structure parameters are listed in Table 2. The most stable configuration (**M1**) has thiophene ring adsorbed on the 4-fold Mo hollow site and the sulfur atom bridges two Mo atoms. During the optimization one of the C−S bonds is broken, and the adsorption energy is −2.82 eV. In **M2** and **M3** the thiophene ring adsorbs molecularly on the Mo hollow sites. On the basis of the computed adsorption energies, **M1** is more stable than **M2** and **M3** (−2.82 vs. −1.74 and −1.62 eV, respectively). It is very interesting to note that the most stable adsorption structure on MoP(001) (**1**) has nearly the same adsorption energy as that on Mo(100) (**M1**).

3.2. Thiophene Adsorption on γ-Mo_2N(100). Cleavage parallel to the (100) plane of the clean γ-Mo_2N exposes unsaturated Mo and N atoms, and 4-fold-type vacancies are created, i.e., octahedral sites (Figure 1b). The Mo_2N(100) plane has a slab of four layers, and the first three layers are allowed

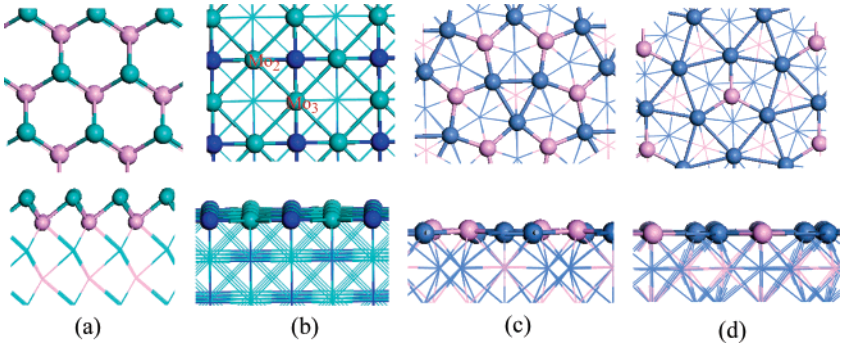

Figure 1. Top and side views of (a) MoP(001), (b) γ-Mo_2N(100), (c) Ni_3P_2-terminated Ni_2P(001), and (d) Ni_3P-terminated Ni_2P(001). Cyan ball for Mo, purple ball for P, deep blue ball for N, and shallow blue ball for Ni.

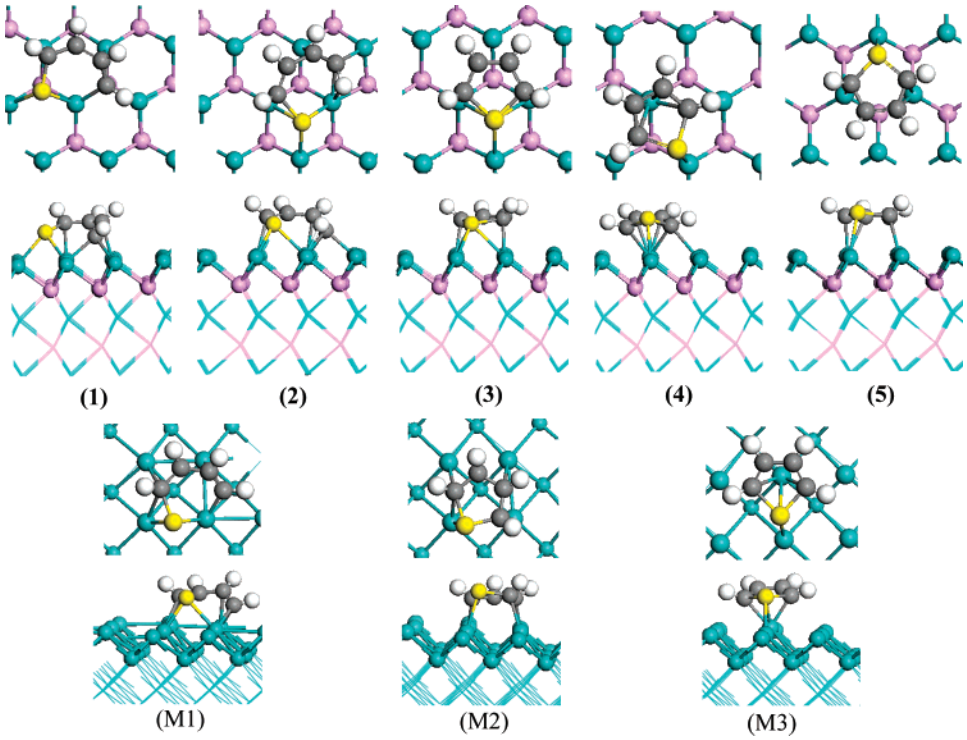

Figure 2. Top and side views of adsorbed thiophene on MoP(001) (**1**−**5**) and on Mo(100) (**M1**−**M3**). Cyan ball for Mo, purple ball for P, yellow ball for S, gray ball for C, and white ball for H.

TABLE 2: Computed Adsorption Energies (E_{ads}, eV) per Molecule and Structural Parameters (d, Å and θ, deg) of Thiophene on MoP(001) and Mo(100)

	E_{ads}[a]	d(S−C)	d(S−Mo)	d(C−Mo)	θ(C_1−S−C_4)
1	−2.78 (−3.87)	1.816; 3.180	2.443; 2.465	2.197−2.284	77.079
2	−2.65 (−3.25)	1.857	2.558; 2.549; 2.470	2.119−2.329	73.973
3	−1.59 (−1.84)	1.864; 1.861	2.637; 2.660; 2.660	2.195; 2.199	94.417
4	−1.55 (−1.81)	1.864; 1.879	2.509	2.284−2.419	83.934
5	−1.51 (−1.77)	1.831; 1.845	2.544	2.234−2.357	92.753
M1	−2.82 (−2.83)	1.833; 3.100	2.562; 2.415	2.180−2.687	77.929
M2	−1.74 (−1.79)	1.832; 1.861	2.499	2.185−2.645	92.720
M3	−1.62 (−1.71)	1.887; 1.851	2.447	2.227−2.440	86.504

[a] Values in parentheses are derived from the DSPP basis set.

to relax, whereas the bottom layer is fixed in their bulk positions. On this surface, there are two individual Mo atoms with different nitrogen coordination numbers, i.e., Mo_2 with two N atoms and Mo_3 with three N atoms. The calculated Mo−Mo and Mo−N bond lengths are 2.954 and 2.087 Å, respectively.

For thiophene adsorption on γ-Mo_2N(100), four models (**6**−**9**) were found in Figure 3, and the computed adsorption energies and structure parameters are given in Table 3. In **6**, thiophene is adsorbed at the N vacancy site and parallel to the (100) surface plane of γ-Mo_2N in the η^3-bonding mode. The S atom points to the Mo_2 site with a distance of 2.558 Å, and the C−S bond lengths are 1.862 and 1.864 Å. The interaction of two Mo_3 sites with C_2 and C_5 results in the rehybridization, and consequently the C_2−H and C_5−H bonds tilt out of the thiophene plane by about 47°, and the C_3−C_4 bond length becomes 1.374 Å as a formal double bond, which is shorter than that in free thiophene (1.430 Å). The C_2−Mo_3 and C_5−Mo_3 distances are 2.262 and 2.263 Å, respectively.

Rotating the adsorbed thiophene in **6** by 45° gives **7** in the η^3-bonding mode. In **7**, the S atom points to the Mo_3 site with

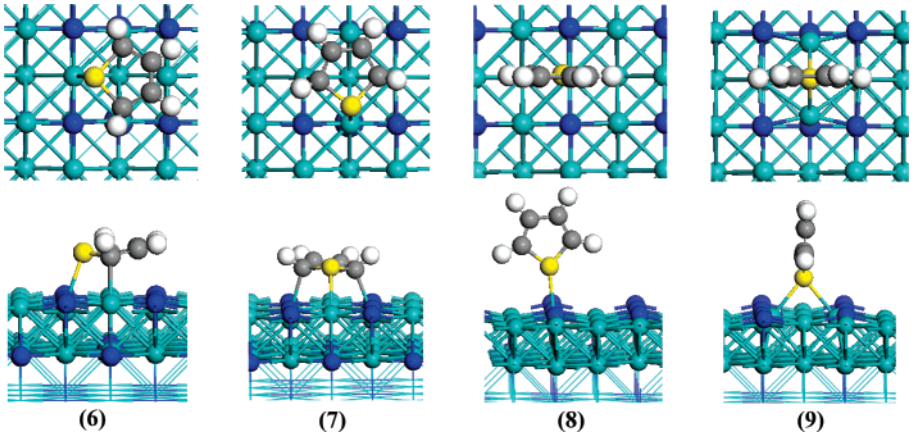

Figure 3. Top and side views of adsorbed thiophene on γ-Mo_2N(100). Cyan ball for Mo, deep blue ball for N, yellow ball for S, gray ball for C, and white ball for H.

TABLE 3: Computed Adsorption Energies (E_{ads}, eV) per Molecule and Structural Parameters (d, Å and θ, deg) of Thiophene on γ-Mo_2N(100)

	E_{ads}[a]	d(S−C)	d(S−Mo)	d(C−Mo)	θ(C_1−S−C_4)
6	−0.59 (−0.74)	1.864; 1.862	2.558	2.262; 2.262	93.877
7	−0.32 (−0.41)	1.850; 1.839	2.529	2.285; 2.298	93.106
8	−0.06 (−0.09)	1.737; 1.738	2.646		92.812
9	−0.02 (−0.04)	1.788; 1.792	2.583; 2.616		90.297

[a] Values in parentheses are derived from the DSPP basis set.

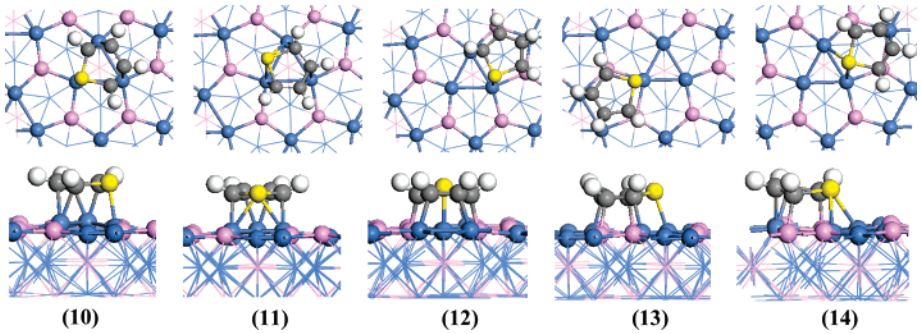

Figure 4. Top and side views of adsorbed thiophene on Ni_3P_2-terminated Ni_2P(001). Blue ball for Ni, shallow purple ball for P, yellow ball for S, gray ball for C, and white ball for H.

a distance of 2.529 Å. The C−S bond lengths are 1.839 and 1.850 Å, and the C_2−Mo_2 and C_5−Mo_2 distances are 2.285 and 2.298 Å, respectively. The C_2−H and C_5−H bonds tilt out of the thiophene plane by about 49°, and the C_3−C_4 bond length becomes 1.389 Å as in **6**.

In **8** and **9**, thiophene is adsorbed perpendicularly to the (100) surface plane via the S lone pair electrons. In **8**, the S atom bonds atop to the Mo_2 site with the S−Mo distance of 2.637 Å, while the S atom in **9** bridges two Mo_3 sites with the S−Mo distances of 2.583 and 2.621 Å, respectively.

As given in Table 3, thiophene adsorption on γ-Mo_2N(100) is weaker than that on MoP(001). The most stable bonding mode **6** has an adsorption energy of only −0.59 eV, which is 21% of that on MoP(001) (**1**), followed by **7** with adsorption energy of −0.32 eV. In addition, two other models (**8** and **9**) are much more unstable due to the small adsorption energies of −0.06 and −0.02 eV.

3.3. Thiophene Adsorption on Ni_2P(001). Scanning tunneling microscopy (STM)[48] and low-energy electron diffraction (LEED)[15] showed that along the [001] direction of bulk Ni_2P there is an alternation of planes with Ni_3P and Ni_3P_2 compositions. A two-plane repeating unit along the [001] direction gives the bulk Ni_2P stoichiometry. Interestingly, for Ni_3P_2- and Ni_3P-terminated surfaces (Figure 1c,d), the surface phosphorus atoms have a 6-fold coordination compared to a bulk coordination number of nine.

Recent theoretical study[49] on the basis of the computed formation energy as a function of the chemical potential shows that the Ni_2P(001) surface prefers to be terminated by Ni_3P_2, but the Ni_3P-terminated surface has comparable thermodynamic stability, and therefore both surfaces can be formed under appropriated experimental conditions. This predication is in agreement with the results of LEED[15] and STM[48] studies of the Ni_2P(001) surfaces. Therefore, both Ni_3P_2- and Ni_3P-terminated surfaces were chosen for thiophene adsorption. The Ni_2P(001) plane has a slab of four layers, and the first three layers are allowed to relax, whereas the bottom layer is fixed in their bulk positions.

On the Ni_3P_2-terminated surface there are five flat adsorption models (**10**−**14**) as shown in Figure 4, and the calculated adsorption energies and structure parameters were given in Table 4. In **10**, the thiophene ring parallels the triangle Ni hollow site and the S atom coordinates atop on one Ni with the S−Ni bond length of 2.270 Å. The S−C bond length extends to 1.789 Å. The C−H bonds tilt away from the surface by about 20°. In comparison with **10**, the thiophene ring in **11** rotates 60° and the S atom bridges two Ni atoms on the triangle Ni hollow site. The S−C bond lengths extend to 1.782 and 1.785 Å, respec-

TABLE 4: Computed Adsorption Energies (E_{ads}, eV) per Molecule and Structural Parameters (d, Å and θ, deg) of Thiophene on $Ni_2P(001)$

	E_{ads}[a]	d(S−C)	d(S−Ni)	d(C−Ni)	d(P−C)	θ(C_1−S−C_4)
			Ni_3P_2-terminated $Ni_2P(001)$			
10	−0.54 (−0.62)	1.789; 1.789	2.270	2.102−2.200		91.453
11	−0.23 (−0.31)	1.782; 1.785	2.447; 2.505	2.077−2.217		93.696
12	0.21 (0.27)	1.879; 1.882	2.318	2.053; 2.052	1.931; 1.936	90.669
13	0.46 (0.41)	1.816; 1.887	2.257	2.006; 2.058	1.933; 1.967	93.513
14	0.93 (0.71)	1.890; 1.892	2.536; 2.571	2.163; 2.163	1.919; 1.920	90.597
			Ni_3P-terminated $Ni_2P(001)$			
15	−1.48 (−1.51)	1.868; 1.806	2.254	2.039−2.160		91.527
16	−0.81 (−0.86)	1.887; 1.829	2.302	2.001−2.131	1.903	91.634
17	−0.25 (−0.27)	1.818; 1.806	2.221; 2.546	2.046; 2.047		92.135
18	−0.12 (−0.15)	1.813; 1.810		2.031−2.112		90.806

[a] Values in parentheses are derived from the DSPP basis set.

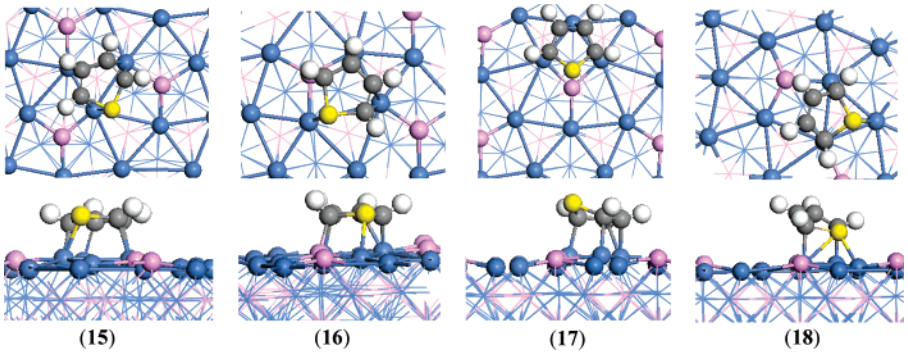

Figure 5. Top and side views of adsorbed thiophene on Ni_3P-terminated $Ni_2P(001)$. Blue ball for Ni, shallow purple ball for P, yellow ball for S, gray ball for C and white ball for H.

tively. The S−Ni bonds (2.447 and 2.505 Å) are slightly longer than that for **10** and the C−H bonds tilt away from the surface by about 28°. In **12**, the thiophene ring caps over the Ni−P pentagon hollow site and the S atom adsorbs atop on one Ni with the S−Ni bond length of 2.318 Å. The S−C bond lengths are 1.879 and 1.882 Å, respectively. Two P−C bonds are formed (1.931 and 1.936 Å). In **13**, the thiophene ring rotates about 120° and the S−C bond lengths are elongated to 1.816 and 1.887 Å, respectively. In **14**, the S atom bridges two Ni atoms on the triangle Ni hollow site and the S−Ni bond lengths are 2.536 and 2.571 Å, respectively.

As given in Table 4, thiophene adsorption on the Ni_3P_2-terminated $Ni_2P(001)$ surface also is weak. The most stable adsorption mode (**10**) has adsorption energy of −0.54 eV, followed by **11** (−0.23 eV). Other adsorption models (**12**−**14**) are thermodynamically unfavorable due to the positive adsorption energy values from 0.21 to 0.93 eV.

On the Ni_3P-terminated surface, four flat adsorption models (**15**−**18**) in Figure 5 are taken into account, and the calculated adsorption energies and structure parameters are listed in Table 4. In **15**, the thiophene ring adsorbs at the triangle Ni hollow site and one C−S bond interacts atop with one Ni, and the S−Ni and C−S bond lengths are 2.263 and 1.868 Å, respectively. In **16**, thiophene adsorbs at the hybrid hollow site constructed by one P atom and three Ni atoms and the S atom coordinates atop with one Ni, and the S−Ni bond length is 2.302 Å. The C−S bonds are elongated to 1.887 and 1.829 Å, respectively. In **17**, thiophene adsorbs aslant at the Ni hollow sites with the S atom bridging two Ni atoms, and the S−Ni bond lengths are 2.221 and 2.546 Å. In **18**, the thiophene ring locates at the hybrid hollow site constructed by one P atom and three Ni atoms and the S atom coordinates atop with one P atom, but the S atom tilts away from the thiophene ring plane by about 25°. The C−S bonds are slightly elongated to 1.813 and 1.810 Å.

As given in Table 4, the most stable adsorption model (**15**) has adsorption energy of −1.48 eV, followed by **16**−**18** with adsorption energies of −0.81, 0.25, and 0.12 eV, respectively. On the basis of calculated adsorption energies of thiophene adsorption on the two surfaces, our results indicate that the Ni_3P-terminated surface is more active than the Ni_3P_2-terminated surface for thiophene adsorption, in line with the recent theoretical study,[49] and LEED and STM results.[15,45]

3.4. Thiophene Dissociation. On the basis of the most stable adsorption model on each surface (**1**, **6**, **10**, and **15**), we are interested in the thermodynamic and kinetic possibility for thiophene dissociation. The computed results for desulfurization are shown in Figures 6 and 7. Beginning with the molecularly adsorbed model, the desulfurization process involves the successive scission of two C−S bonds. We have used **I** for the adsorption state with one broken C−S bond, and **II** for that with two broken C−S bonds.

Since one C−S bond is already broken on MoP(001), it is only necessary to break the second C−S bond for desulfurization. The adsorption structure **1** (also **1-I**) with one broken C−S bond is highly exothermic (−2.78 eV), and the break of the second C−S (from **1** to **1-II**) bond with the formation of adsorbed sulfur and open-chain C_4H_4 unit from **1** is exothermic by 1.28 eV, and the energy barrier is 1.02 eV (Figure 7), indicating that thiophene can easily dissociate on MoP(001) both kinetically and thermodynamically. Such a phenomenon is also observed for thiophene adsorption on metal and Mo carbide surfaces.[31,50] For comparison, we also have computed the dissociation of the second C−S bond of adsorbed thiophene on Mo(100). The corresponding barrier is 0.48 eV, and the reaction is exothermic by 1.77 eV, indicating that Mo(100) is more active for C−S bond dissociation than MoP(001). This effect can be explained by the downshift of the metal d-band caused by the underneath P atoms.[45]

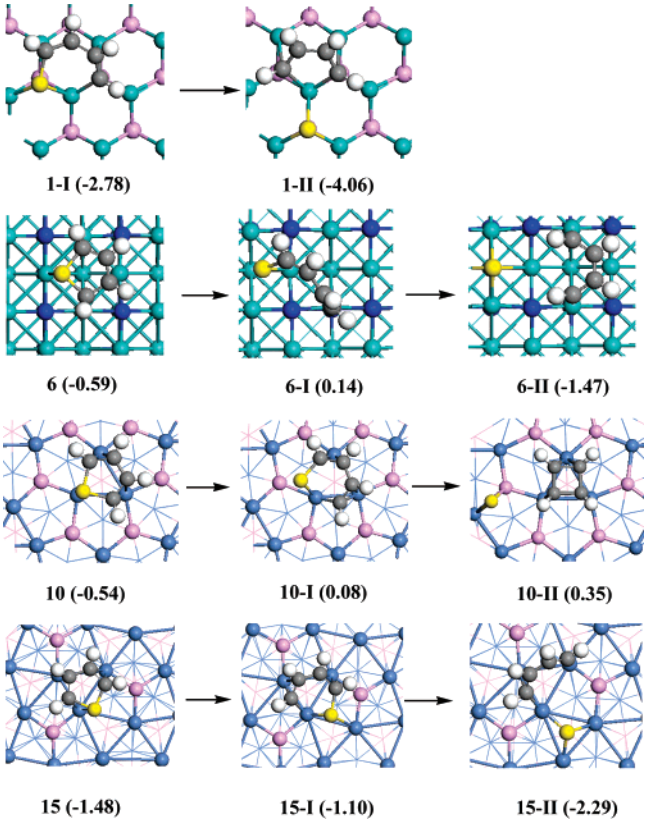

Figure 6. Calculated energy (eV) schemes for the dissociation of the C−S bonds of adsorbed thiophene on the MoP(001), γ-Mo_2N(100), and Ni_2P(001) surfaces. **I** indicates the adsorption state with one broken C−S bond, while **II** indicated that for two broken C−S bonds. Cyan ball for Mo, purple ball for P, deep blue ball for N, shallow blue ball for Ni, yellow ball for S, gray ball for C, and white ball for H.

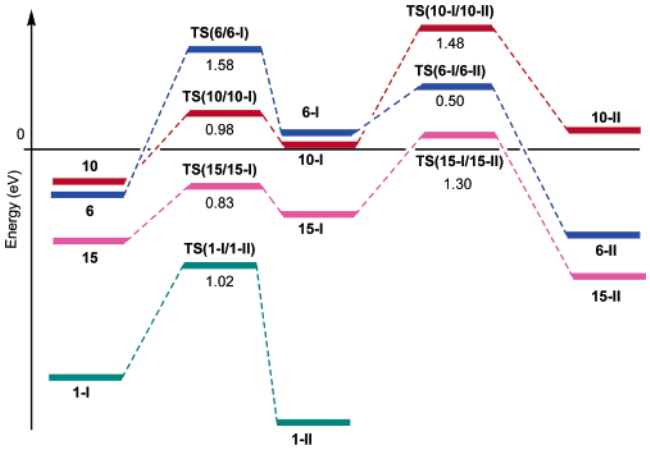

Figure 7. The calculated activation energy barriers of thiophene dissociation associated with the desulfurization of thiophene on these catalysts surfaces.

For thiophene dissociation on γ-Mo_2N(100), the break of the first C−S bond (**6-I**, Figure 6) is endothermic by 0.73 eV, compared with the molecularly adsorbed thiophene **6**, and the corresponding energy barrier is 1.58 eV. However, the break of the second C−S bond with the formation of adsorbed sulfur and the open-chain C_4H_4 unit is highly exothermic by 1.61 eV, and the energy barrier is 0.50 eV. The cleavage of both C−S bonds from **6** to **6-II** is exothermic by 0.88 eV. That the first C−S bond cleavage on the γ-Mo_2N(100) surface is difficult both kinetically and thermodynamically is in reasonable agreement with the experiment observation,[14] which shows that the adsorbed thiophene has a strong interaction with the Mo_2N/γ-Al_2O_3 catalyst and does not sulfide the surface at temperatures below 673 K. While in the presence of H_2 the surface of the Mo_2N/γ-Al_2O_3 catalyst can be partially sulfided by thiophene at a temperature as low as 373 K, and the adsorbed thiophene decomposes simultaneously.

On the Ni_3P_2-terminated Ni_2P(001) surface, the cleavage of the first C−S bond (from **10** to **10-I**) is endothermic by 0.62 eV, and the breaking of the second C−S bond also is endothermic by 0.27 eV. To break two C−S bonds on the Ni_3P_2-terminated Ni_2P(001) surface costs 0.89 eV. The corresponding energy barriers of first and second C−S bonds are 0.98 and 1.48 eV, respectively. It should be noted that on the surface a cyclic C_4H_4 unit instead of an open-chain C_4H_4 unit is formed.

Compared with the Ni_3P_2-terminated Ni_2P(001) surface, the breaking of the first C−S bond (from **15** to **15-I**) is endothermic by 0.38 eV with the barrier of 0.81 eV, but the break of the second C−S bond is exothermic (−1.19 eV) and the barrier is 1.32 eV. Therefore, it should be relatively easy to break two C−S bonds on the Ni_3P-terminated Ni_2P(001) surface. Experimentally, C−S bond scission on this catalyst at 190 K was observed by IR spectra.[18,27−29] Thus, our results are reasonably consistent with experiment. Both indicate that the dissociation of thiophene on the Ni_2P(001) surface is a relatively facile reaction.

4. Conclusions

Thiophene adsorption on the MoP(001), γ-Mo_2N(100), and Ni_2P(001) surfaces has been investigated at the density functional theory level of theory. On MoP(001), the most stable adsorption model (**1**) with one broken C−S bond is exothermic, indicating the strong interaction and activation of thiophene, and the successive dissociation of the second C−S bond is also exothermic. In contrast, thiophene adsorption (**6**) on γ-Mo_2N(100) is molecular and moderate, and weaker than that on MoP(001). In addition, the dissociation of the first C−S bond on γ-Mo_2N(100) is endothermic, but that of the second C−S bond is exothermic.

On the Ni_3P_2-terminated Ni_2P(001) surface, the most stable adsorption model (**10**) is molecular, and the dissociation of the first and second C−S bonds is endothermic. On the Ni_3P-terminated Ni_2P(001) surface, which is higher in energy, the most stable adsorption model (**15**) is also molecular, the dissociation of the first C−S bond is slightly endothermic, but that of the second C−S bond is exothermic. This indicates the difference of two surfaces in thiophene adsorption and activation.

Acknowledgment. This work has been supported by the National Nature Science Foundation of China (20473111, 20590360, and 20573127). We also thank Dr. P. Liu for helpful discussion (Brookhaven National Laboratory).

References and Notes

(1) (a) Chen, J. G. G. *Chem. Rev.* **1996**, *96*, 1447. (b) Hwu, H. H.; Chen, J. G. G. *Chem. Rev.* **2005**, *105*, 185. (c) Rodriguez, J. A. *J. Phys. Chem. B* **1997**, *101*, 7524. (d) Tarbuck, T. L.; McCrea, K. R.; Logan, J. W.; Heiser, J. L.; Bussell, M. E. *J. Phys. Chem. B* **1998**, *102*, 7845. (e) St. Clair, T. P.; Oyama, S. T.; Cox, D. F. *Surf. Sci.* **2002**, *511*, 294.

(2) (a) Zonnevylle, M. C.; Hoffmann, R.; Harris, S. *Surf. Sci.* **1988**, *199*, 320. (b) Satterfield, C. N. *Heterogeneous Catalysis in Industrial Practice*; Mc-Graw Hill: New York, 1991.

(3) (a) Rodriguez, J. A.; Dvorak, J.; Jirsak, T. *J. Phys. Chem. B* **2000**, *104*, 11515. (b) Oyama, S. T. *Catal. Today* **1992**, *15*, 179.

(4) (a) Sajkowski, D. J.; Oyama, S. T. *Appl. Catal., A* **1996**, *134*, 339. (b) Nagai, M.; Goto, Y.; Ishii, H.; Omi, S. *Appl. Catal., A* **2000**, *192*, 189.

(5) Saito, M.; Anderson, R. B. *J. Catal.* **1980**, *63*, 438.

(6) Kijima, R.; Aika, K. *Appl. Catal., A* **2001**, *219*, 141.

(7) Woo, H. C.; Park, K. Y.; Kim, Y. G.; Nam, In-Sik.; Chung, J. S.; Lee, J. S. *Appl. Catal.* **1991**, *75*, 267.
(8) Oyama, S. T.; Yu, C. C.; Ramanathan, S. *J. Catal.* **1999**, *184*, 535.
(9) Rodriguez, J. A.; Dvorak, J.; Jirsk, T. *Surf. Sci.* **2000**, *457*, L413.
(10) Markel, J.; Van Zee, J. W. *J. Catal.* **1990**, *126*, 643.
(11) Lucy, T. E.; St. Clair, T. P.; Oyama. S. T. *J. Mater. Res.* **1998**, *13*, 2321.
(12) Schwartz, V.; Da Silva, V. T.; Oyama, S. T. *J. Mol. Catal. A* **2000**, *163*, 251.
(13) Rousseau, G. B.; Bovet, N.; Johnston, S. M.; Lennon, D.; Dhanak, V.; Kadodwala, M. *Surf. Sci.* **2002**, *511*, 190.
(14) Wu, Z.; Li, C.; Wei, Z.; Ying, P.; Xin, Q. *J. Phys. Chem. B* **2002**, *106*, 979.
(15) Kanama, D.; Oyama, S. T.; Otani, S.; Cox, D. F. *Surf. Sci.* **2004**, *552*, 8.
(16) Oyama, S. T. *J. Catal.* **2003**, *216*, 343.
(17) Sawhill, S. J.; Phillips, D. C.; Bussell, M. E. *J. Catal.* **2003**, *215*, 208.
(18) Layman, K. A.; Bussell, M. E. *J. Phys. Chem. B* **2004**, *108*, 15791.
(19) Rodriguez, J. A.; Kim, J. Y.; Hanson, J. C.; Sawhill, S. J.; Bussell, M. E. *J. Phys. Chem. B* **2003**, *107*, 6276.
(20) (a) Korányi, T. I. *Appl. Catal., A* **2002**, *237*, 1. (b) Sun, F.; Wu, W.; Wu, Z.; Guo, J.; Wei, Z.; Yang, Y.; Jiang, Z.; Tian, F.; Li, C. *J. Catal.* **2004**, *228*, 298.
(21) (a) Oyama, S. T.; Wang, X.; Lee, Y. K.; Bando, K.; Requejo, F. G. *J. Catal.* **2002**, *210*, 207. (b) Stinner, C.; Prins, R.; Weber, T. *J. Catal.* **2001**, *202*, 187.
(22) Li, W.; Dhandapani, B.; Oyama, S. T. *Chem. Lett.* **1998**, *27*, 207.
(23) Stinner, C.; Prins, R.; Weber, T. *J. Catal.* **2000**, *191*, 438.
(24) Phillips, D. C.; Sawhill, S. J.; Self, R.; Bussell, M. E. *J. Catal.* **2002**, *207*, 266.
(25) (a) Clark, P.; Wang, X.; Oyama, S. T. *J. Catal.* **2002**, *207*, 256. (b) Wu, Z.; Sun, F.; Wu, W.; Feng, Z.; Liang, C.; Wei, Z.; Li, C. *J. Catal.* **2004**, *222*, 41.
(26) (a) Clark, P.; Li, W.; Oyama, S. T. *J. Catal.* **2001**, *200*, 140. (b) Oyama, S. T.; Clark, P.; Wang, X.; Shido, T.; Iwasawa, Y.; Hayashi, S.; Ramallo-López, J. M.; Requejo, F. G. *J. Phys. Chem. B* **2002**, *106*, 1913.
(27) (a) Wang, X.; Clark, P.; Oyama, S. T. *J. Catal.* **2002**, *208*, 321. (b) Stinner, C.; Tang, Z.; Haouas, M.; Weber, T.; Prins, R. *J. Catal.* **2002**, *208*, 456.
(28) Oyama, S. T.; Wang, X.; Requejo, F. G.; Sato, T.; Yoshimura, Y. *J. Catal.* **2002**, *209*, 1.
(29) Oyama, S. T.; Wang, X.; Lee, Y. K.; Chun. W. J. *J. Catal.* **2004**, *221*, 263.
(30) (a) Robinson, W. R. A. M.; van Gastel, J. N. M.; Korányi, T. I.; Eijsbouts, S.; van Veen, J. A. R.; de Beer, V. H. J. *J. Catal.* **1996**, *161*, 539.
(31) (a) Milligan, P. K.; Murphy, B.; Lennon, D.; Cowie, B. C. C.; Kadodwala, M. *J. Phys. Chem. B* **2001**, *105*, 140. (b) Terada, S.; Yokoyama, T.; Sakano, M.; Imanishi, A.; Kitajima, Y.; Kiguchi, M.; Okamoto, Y.; Ohta, T. *Surf. Sci.* **1998**, *414*, 107. (c) Morin, C.; Eichler, A.; Hirschl, R.; Sautet, P.; Hafner, J. *Surf. Sci.* **2003**, *540*, 474.
(32) Khan, N. A.; Hwu, H. H.; Chen, J. G. G. *J. Catal.* **2002**, *205*, 259.
(33) Venezia, A. M.; Parola, V. La.; Nicoli, V.; Deganello, G. *J. Catal.* **2002**, *212*, 56.
(34) Smelyansky, V.; Hafner, J.; Kresse, G. *Phys. Rev. B* **1998**, *58*, R1782.
(35) Hada, K.; Tanabe, J.; Omi, S.; Nagai, M. *J. Catal.* **2002**, *207*, 10.
(36) (a) Payne, M. C.; Allan, D. C.; Arias, T. A.; Joannopoulos, J. D. *Rev. Mod. Phys.* **1992**, *64*, 1045. (b) Milman, V.; Winkler, B.; White, J. A.; Pickard, C. J.; Payne, M. C.; Akhmataskaya, E. V.; Nobes, R. H. *Int. J. Quantum Chem.* **2000**, *77*, 895.
(37) (a) Delley, B. *J. Chem. Phys.* **1990**, *92*, 508. (b) Delley, B. *J. Phys. Chem.* **1996**, *100*, 6107. (c) Delley, B. *J. Chem. Phys.* **2000**, *113*, 7756.
(38) Hammer, B.; Hansen, L. B.; Nørskov, J. K. *Phys. Rev. B* **1999**, *59*, 7413.
(39) Liu, P.; Rodriguez, J. A. *Catal. Lett.* **2003**, *91*, 247.
(40) Vanderbilt, D. *Phys. Rev. B* **1990**, *41*, 7892.
(41) Monkhorst, H. J.; Pack, J. D. *Phys. Rev. B* **1976**, *13*, 5188.
(42) Oyama, S. T.; Clark, P.; Teixeira da, V. L. S.; Lede, E. J.; Requejo, F. G. *J. Phys. Chem. B* **2001**, *105*, 4961.
(43) (a) Gouin, X.; Marchand, R.; L'Haridon, P.; Laurent, Y. *J. Solid State Chem.* **1994**, *109*, 175. (b) Frapper, G.; Pélissier, M.; Hafner, J. *J. Phys. Chem. B* **2000**, *104*, 11972.
(44) Rundqvist, S. *Acta Chem. Scand.* **1962**, *16*, 992.
(45) Liu, P.; Rodriguez, J. A.; Asakura, T.; Gomes, J.; Nakamura, K. *J. Phys. Chem. B* **2005**, *109*, 4575.
(46) Liu, P.; Rodriguez, J. A. *J. Am. Chem. Soc.* **2005**, *127*, 14871.
(47) Feng, Z.; Liang, C.; Wu, W.; Wu, Z.; van Santen, R. A.; Li, C. *J. Phys. Chem. B* **2003**, *107*, 13698.
(48) Golam Moula, M.; Suzuki, S.; Chun, W. J.; Otani, S.; Oyama, S. T.; Asakura, K. *Chem. Lett.* **2006**, *35*, 90.
(49) Li, Q.; Hu, X. *Phys. Rev. B* **2006**, *74*, 035414.
(50) Liu, P.; Rodriguez, J. A.; Muckerman, J. T. *J. Phys. Chem. B* **2004**, *108*, 15662.